International Journal of Plasticity 43 (2013) 116–127

Contents lists available at SciVerse ScienceDirect

International Journal of Plasticity

journal homepage: www.elsevier.com/locate/ijplas

A molecular dynamics study on the orientation, size, and dislocation confinement effects on the plastic deformation of Al nanopillars

S. Xu [a,b], Y.F. Guo [a,*], A.H.W. Ngan [b]

[a] Institute of Engineering Mechanics, Beijing Jiaotong University, Beijing 100044, China
[b] Department of Mechanical Engineering, The University of Hong Kong, Pokfulam Road, Hong Kong

ARTICLE INFO

Article history:
Received2August2012
Received in final revised form 30 October 2012
Available online 19 November 2012

Keywords:
B. Metallic materials
A. Dislocations
A. Microstructures
Molecular dynamics

ABSTRACT

Molecular dynamics are employed to simulate the compression process of Al nanopillars with different orientations. The simulations show that the initial dislocations always nucleate at free surfaces but the compression orientation plays a decisive role in the subsequent microstructural evolution and stress–strain response of the pillars. For higher symmetry orientations of [001] and [111], frequent dislocation interactions make the dislocation-starvation state not easily achievable, and the more mean-field interaction condition leads to less serrated stress–strain response. Lower symmetry orientations behave in the opposite way. Simulation of the presence of a rigid coating on the pillar's surface also shows that dislocations are trapped by the coating with smooth strain-hardening after the initial dislocations are generated. The results show that whether the dislocation-starvation state can be achieved is a crucial factor governing the stress–strain response of small crystals.

1. Introduction

It is well known that the deformation behavior of metallic materials with dimensions down to the sub-micrometer scale is very different from that of the corresponding bulk materials. In recent years, the mechanical behavior exhibited by micrometer or nanometer sized material volumes has attracted increasing attention and small-scale compression tests on single crystalline metal micropillars have consistently shown a very prominent strong size effect in which the yield strength increases significantly on decreasing sample size (Dimiduk et al., 2007; Greer and Nix, 2006; Greer et al., 2005; Jang et al., 2011; Kim et al., 2012; Korte et al., 2011; Ng and Ngan, 2008; Uchic et al., 2004, 2009; Wang et al., 2012; Yoo et al., 2012). Furthermore, their plastic deformation is in general a jerky and stochastic process with sporadic occurrence of sudden strain bursts.

As it is well known, Uchic et al. (2004) reported measurements of plastic yielding for single crystals of micrometer-sized dimensions for three different types of metals. They found that large strain bursts occurred for the 5-μm-diameter samples with [123] and [134] orientations. Subsequently, Dimiduk et al. (2007) studied the size-affected single-slip behavior of [269]-oriented Ni microcrystals. They suggested that dislocation behavior is stochastic for characteristic dimensions below ~20 μm, and size-affected changes in dislocation mechanisms may be more important than gradient-induced storage of geometrically-necessary dislocations in determining the stress. In Ng et al.'s experiments on $[3\bar{1}5]$-oriented micron-sized aluminum pillars (Ng and Ngan, 2008), the jerky deformation and the statistical distributions of the sizes of the bursts were analyzed. It was found that the burst size increased with stress in an approximately exponential manner, whereas the dislocation density of the micro-pillars did not grow significantly after severe deformation. More recently, Wang et al. (2012)

* Corresponding author. Tel.: +86 10 51682094.
E-mail address: yfguo@bjtu.edu.cn (Y.F. Guo).

0749-6419/$ - see front matter © 2012 Elsevier Ltd. All rights reserved.
http://dx.doi.org/10.1016/j.ijplas.2012.11.002

performed *in situ* transmission electron microscope compression testing of $[2\bar{2}0]$-oriented Al pillars, and two different mechanisms underlying the large strain bursts were found. For small pillars, the bursts were characterized by very high collapse stresses and a nearly dislocation-free post-collapse microstructure. For larger pillars, the bursts resulted from the reconstruction of jammed dislocation configurations, featuring relative low stress levels and retention of dislocation network after bursts. Furthermore, Kim et al. (2012) reported that the difference between attained flow stresses in tension vs. compression of Mo nano-pillars depends on crystallographic orientation and sample size. They observed that when deformed along pillar axes in [001] orientation, the compressive flow stresses are higher than tensile ones, and vice versa in [011] orientation, as consistent with bulk Mo. They hypothesized that in smaller Mo nano-pillars, screw dislocations play a lesser role in governing plasticity, and the observed size-dependent tension–compression asymmetry is likely due to the relative shortage of screw dislocations. From above experiments, the jerky and stochastic deformation behavior has been observed in small-scale pillars with different orientations due to the strong size effect. However, the relationship between the orientation and the deformation behavior has never been discussed.

To better understand these unusual deformation behaviors, computer simulations based on 3D dislocation dynamics (Akarapu et al., 2010; El-Awady et al., 2011; Liu et al., 2009; Rao et al., 2008; Wang et al., 2009) and molecular dynamics (Cao and Ma, 2008; Diao et al., 2006; Horstemeyer et al., 2001; Kang and Cai, 2010; Li and Yang, 2009; Park et al., 2006; Rabkin et al., 2007; Weinberger et al., 2012a,b; Zhu et al., 2008; Zuo and Ngan, 2006; Zuo et al., 2005) have been employed to study the plastic deformation of small pillars. For example, Horstemeyer et al. (2001) revealed that slip nucleates at free surfaces, and a power-law relationship between the flow stress and the volume-to-surface area ratio of the sample was reported. Based on simulations of Ni_3Al single crystal, Zuo and Ngan (2006), Zuo et al. (2005) proposed a survivability theory for homogeneous dislocation generation to predict the incipient plasticity behavior of real-sized micro-pillars in real time scales. Rabkin et al. (2007) suggested that dislocation nucleation at the surface occurs at a critical strain, where the local strain has contributions from both homogeneous elastic strain and an atomic-level thermal strain, and this model explains the observed temperature dependence of yield stress in nanopillars. Moreover, Li and Yang (2009) showed that the deformation mechanisms during compression of Ni nanopillars are characterized by massive dislocation activities within a single slip system and a nanoscale deformation twinning process in an octal slip system, and the size and temperature effects in single slip-oriented nanopillars were interpreted by a dislocation dynamics-based model considering the nucleation of incipient dislocations. More recently, Liu and Shen (2012) studied the mechanical behaviors of silicon nanowires with different axial orientations under tension at low temperature. The snapshots of the deformation processes demonstrated different failure responses for different orientated nanowires. Detailed analyses revealed that the initial yielding behaviors of $\langle 110 \rangle$ and $\langle 100 \rangle$ silicon nanowires are due to dislocation emission and crystal-to-amorphous transition, respectively. Weinberger et al. (2012b) used the transition state theory to estimate the strength in gold nanowires at experimentally relevant time scales, and concluded that the strength of pristine wires is controlled by heterogeneous dislocation nucleation at free surfaces. The nucleation stress was found to depend on the line length and orientation of the dislocations.

We have found that all above experimental and simulated analysis have mostly focused on size effect on the yielding strength and the deformation behaviors, yet a comprehensive understanding of the mechanism of jerky deformation in small pillars is still lacking. Greer and Nix (2006) and Greer et al. (2005) proposed a dislocation starvation hypothesis which stipulates that if the rate of dislocation escape from a free surface is greater than that of dislocation multiplication in a small crystal, then a "dislocation starvation" condition would arise, in which the crystal is continually kept in a state depleted of mobile dislocations, and plasticity is only facilitated by the nucleation of new dislocations at a high stress. Such a starvation condition has been observed directly by *in situ* electron microscopy (Shan et al., 2008) in nano-pillars. Also, as a corollary of the starvation theory, the jerky nature of the deformation should be alleviated when dislocations are confined inside the deforming crystal by external means, and experimental results indeed revealed such a phenomenon in Al micro-pillars with a coating or an internal grain boundary which served to trap the dislocations (El-Awady et al., 2011; Kunz et al., 2011; Ng and Ngan, 2009a,b).

In this study, the compression of Al nanopillars with different orientations and sizes is simulated by molecular dynamics. The mechanisms of jerky deformation in nanopillars are clearly observed and analyzed by considering the influence of crystallographic orientation and size of the pillars.

2. Method and simulation procedures

In the simulations, the model used was a pristine single crystal with a length-to-diameter ratio of 2:1. The simulated systems contained approximately 10^4 to 10^7 Al atoms, depending on their size. We examined cylinders with the long axis parallel to the [001], [111], [112] and $[\bar{2}\bar{6}5]$-directions in the fcc lattice. The simulations were performed in constant NVT ensemble with a velocity-Verlet integrator and a time step of 3.5×10^{-15} s. Temperature was controlled at 10 and 300 K by the Nosé–Hoover thermostat. Voter–Chen's embedded atom method potentials for Al (Voter and Chen, 1987) and the molecular dynamics program LAMMPS (Plimpton, 1995) was employed in the simulations. The Atomeye software (Li, 2003) was used for visualizing the evolution of the atomistic structures.

In a first step, the perfect crystal arrangement of the simulated pillar was relaxed for 70 ps (20,000 time steps) at zero force to minimize the potential energy. After that, uniaxial compression was performed along the *z*-direction (the long axis). This was done in a displacement-controlled manner, by imposing compressive displacements to atoms along the *z*-direction

that varied linearly from zero at the bottom to a maximum value at the top layer. Then the system was relaxed for 3.5 ps before the next increment of compressive displacement was applied, and the strain rate in the simulation was set as 6×10^8/s. During this step, only the z-component displacements of the bottom-most and top-most layer were fixed while all other degrees of freedom were not controlled. The simulations were carried out until the maximal strain reached about 20%. At each loading step, the configuration of the atoms, the atomic energy and stress conditions were recorded for further analysis.

3. Results and discussion

3.1. Plastic deformation mechanisms for different nanopillar orientations

Fig. 1 shows the stress–strain response of nanopillars with different orientations. It can be seen that the nanopillars with different orientations show rather different plastic deformation behaviors. After an initial yield peak, the plastic flow stress of the [001] and [111]-oriented nanopillars shown in Fig. 1a and b fluctuate within a certain range, while that of the [112] and [$\bar{2}\bar{6}5$]-oriented nanopillars appears to fluctuate much more severely. As shown in Fig. 1c and d, after the initial yield peak, the flow stress of the [112] and [$\bar{2}\bar{6}5$]-oriented nanopillars builds up again to a second and third stress peak.

To better understand the different plasticity behaviors observed in Fig. 1, the microstructure evolution during compression was carefully studied. Fig. 2 represents the microstructural evolution of the [001]-oriented nanopillar under compression. Snapshots in Fig. 2a–h are related to the tagged points (A–H) in Fig. 1a. In this and subsequent figures, we illustrate the deformation in the pillars using the Common Neighbor Analysis (CNA) (Honeycutt and Andersen, 1987). For clarity, atoms on perfect fcc lattice are not shown in the plot, and atoms on hcp lattice are shown in blue while those of other defects such as surface and dislocation cores are shown in red. From the snapshots, we can see that stacking faults bounded by partial dislocations on four different {111} planes nucleate almost at the same time in Fig. 2a, and this results in a sharp drop in stress at point A. It should be noted that we can only observe the leading partials of the initial loops in Fig. 2a, as the trailing partial is not nucleated until the stacking faults on different slip planes intersect each other (Fig. 2b and c). The subsequent emission and glide of the trailing partials cause the stacking faults to shrink in width. At a later stage, Lomer–Cottrell barriers and micro-twins are produced by stacking faults intersection (Fig. 2d and e), and these block the dislocation migration and

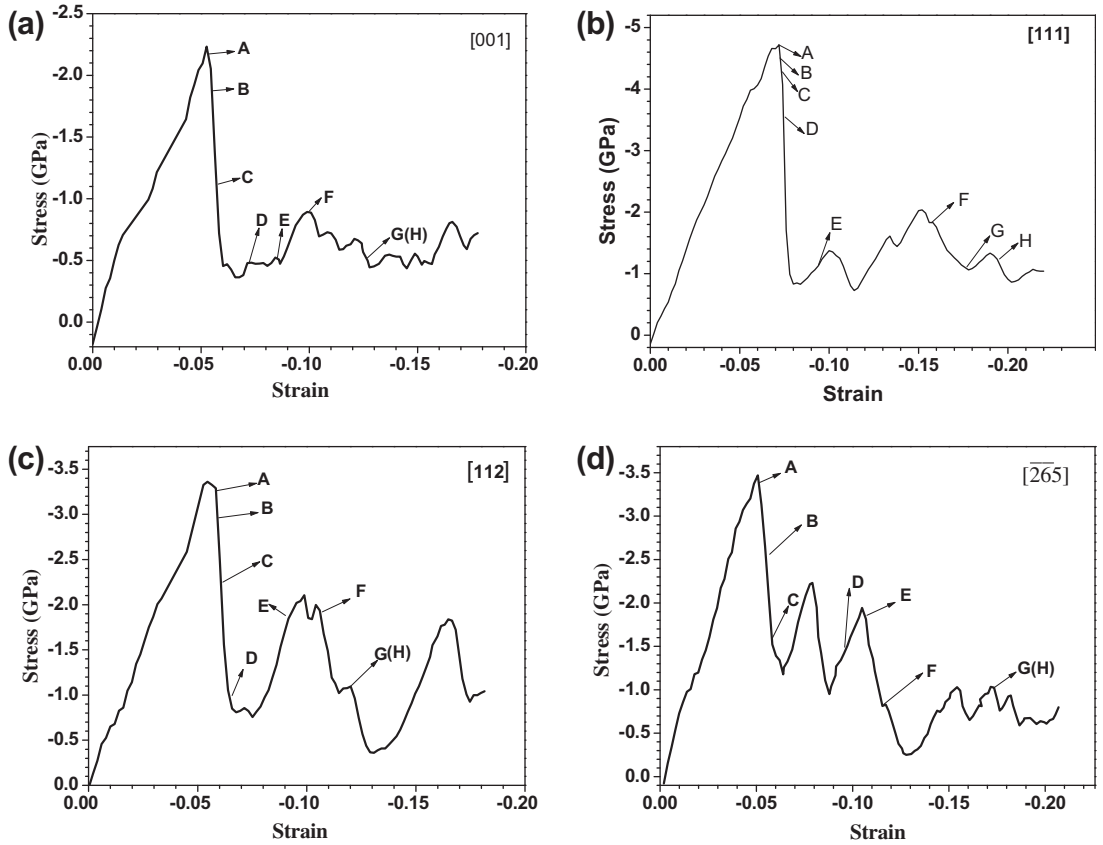

Fig. 1. Stress–strain curves for nanopillars with different orientations (D = 16 nm, T = 10 K).

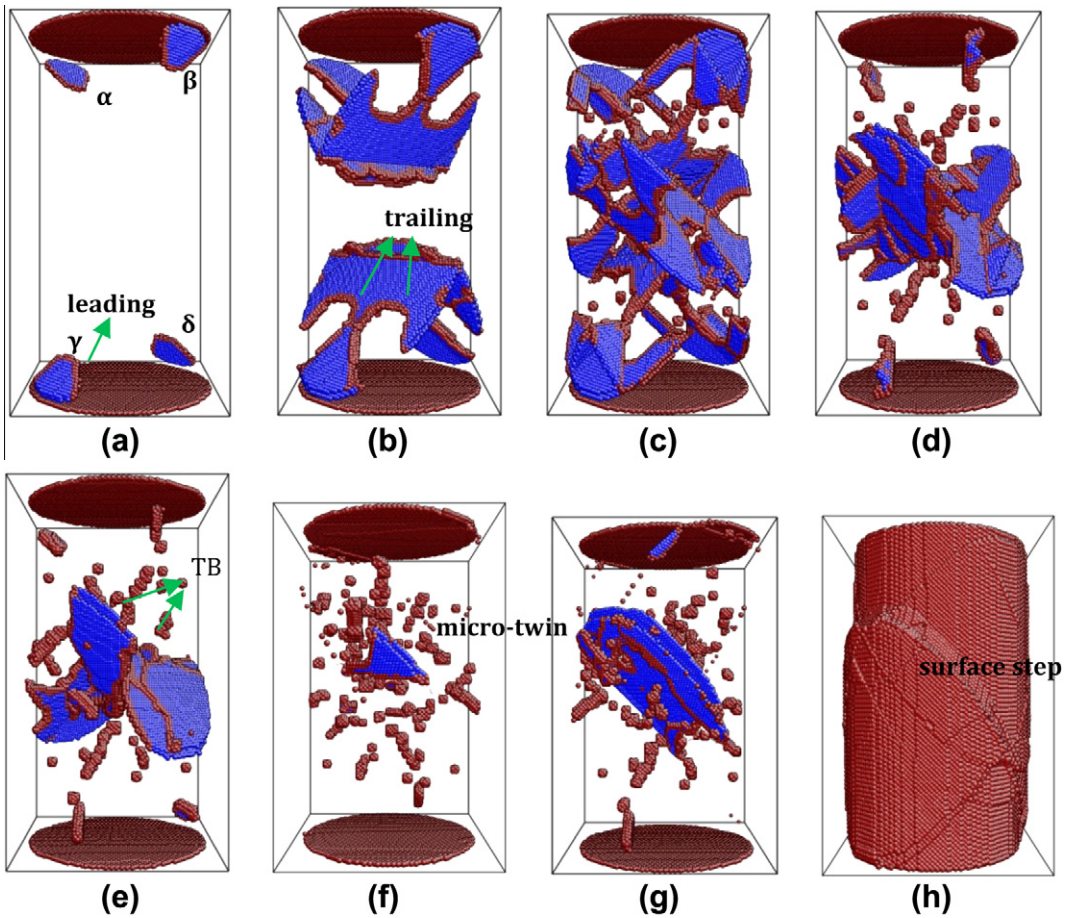

Fig. 2. Snapshots show for the microstructure evolution of the [0 0 1]-oriented nanopillar under compression (T = 10 K). Atoms on the side-surface are not shown in (a–g). Stacking faults bounded by partial dislocations (a) and micro-twins (e) are main plastic deformation mechanisms.

correspond to the flow near points D and E in Fig. 1a. Moreover, as we can see in Fig. 2f, Lomer–Cottrell barriers can be overcome as strain increases, and stacking faults bounded by partial dislocations tend to annihilate at the surface. Small twin boundaries (TB) are left in the pillar, and the pillar returns to a nearly defect-free state. With further compression, small twin boundaries grow across the whole pillar as shown in Fig. 2g, and finally surface steps are left (Fig. 2h).

It is worth noting that previous work by Park et al. (2006) and Cao and Ma (2008) has shown that there is no dislocation-locking in fcc nanowires under compression at 300 K. This difference indicates the importance of temperature when examining the plastic deformation mechanism of nanopillars. As a result, 300 K compression simulations of different oriented nanopillars with D = 8 nm were also performed in the current work. From Fig. 3, a similar strong orientation effect just as compression simulations at low temperature can be seen: the [1 1 2] and [$\bar{2}$65]-oriented nanopillars exhibit a much more serrated stress–strain response than the [0 0 1] and [1 1 1]-oriented nanopillars. However, the stress–strain curve at 300 K has more fluctuations due to thermal activation, and the yield stress is lower than that at low temperature. Moreover, we examined the microstructure evolution for all four different oriented nanopillars at 300 K, and compared them with the results at 10 K. It is found that the deformation mechanisms are not affected by temperature, except for a small difference for the [0 0 1]-oriented sample. Fig 4 shows the microstructure evolution of the [0 0 1]-oriented nanopillar under compression at 300 K. Snapshots in Fig. 4a–e are related to the tagged points (A–E) in Fig. 3a, except that the effects of thermal fluctuations were removed by conjugate gradient relaxation. From Fig. 4a–c, it can be seen that slip events nucleate one-by-one on α, β and γ plane, where stacking faults are bounded by partial dislocations. With the applied strain increasing, the stacking faults on α plane transform into a micro-twin by new partial dislocations nucleating on adjacent $\langle 1\,1\,1\rangle$ planes (Fig. 4c and d). On the contrary, the partial dislocations on β and γ plane annihilate at the free surface, and stacking faults on these planes also disappear (Fig. 4c–e). Compared with the results at 10 K, no dislocation-locking is formed at 300 K. Due to the effects of thermal fluctuation, slip on different {1 1 1} planes no longer nucleates simultaneously at 300 K, and this reduces the probability of stacking faults intersection between different planes. As a result, some stacking faults bounded by partial dislocations easily run out of the pillar before interaction, and dislocation-locking events are much more difficult to form at higher temperatures.

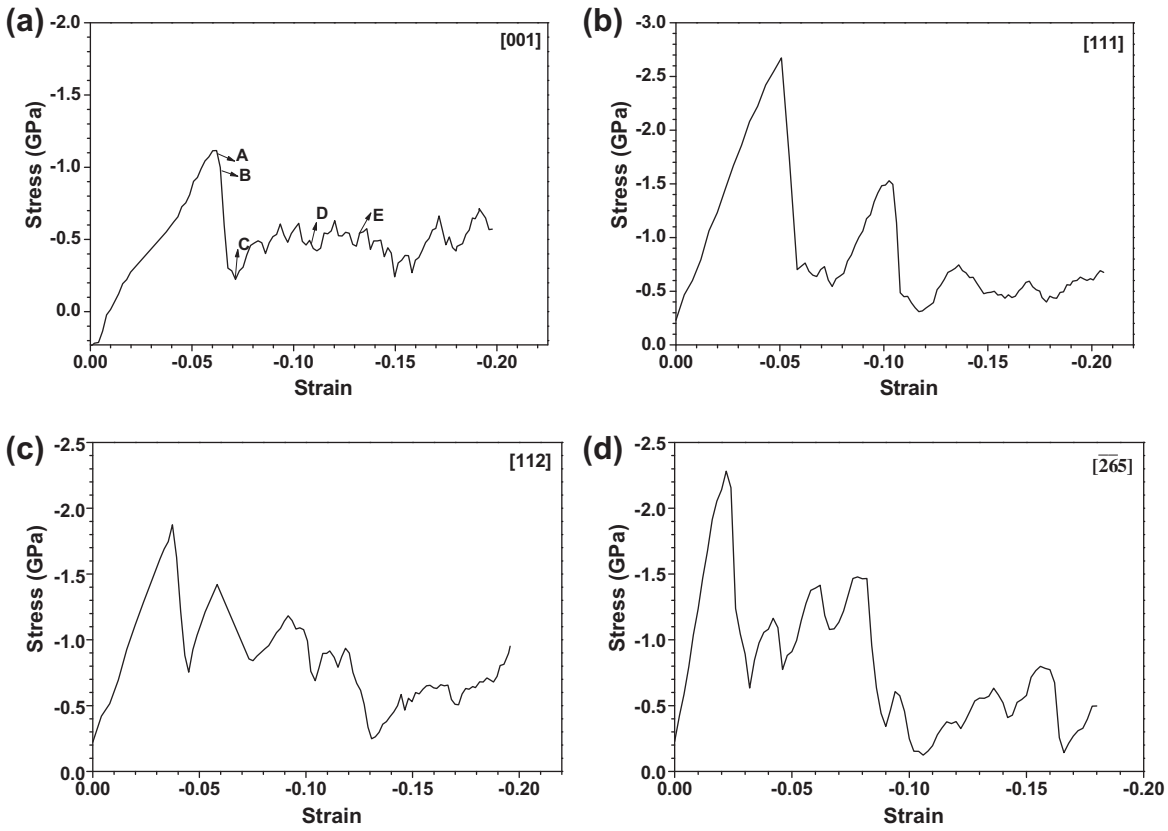

Fig. 3. Stress–strain curves for nanopillars with different orientations (D = 8 nm, T = 300 K).

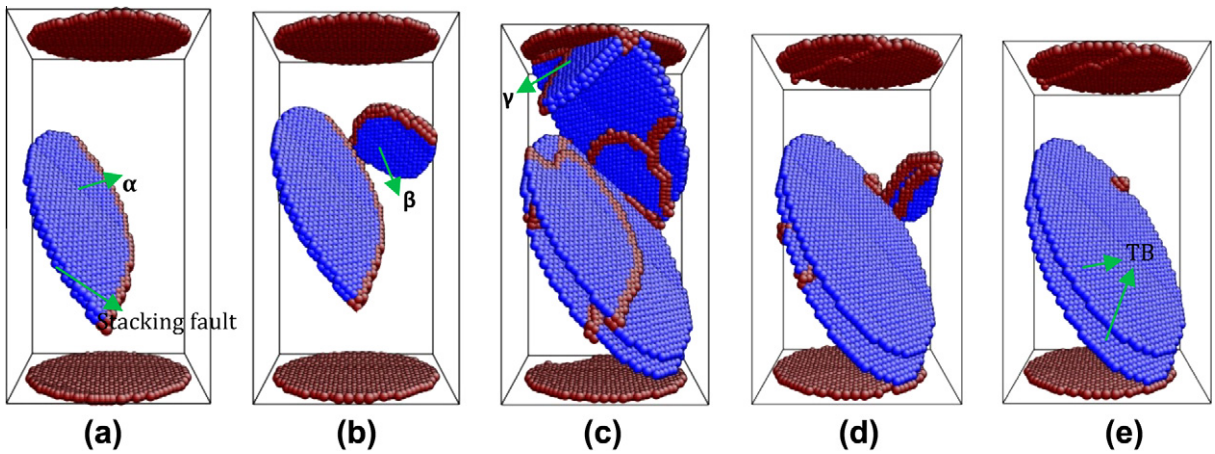

Fig. 4. Snapshots showing the microstructure evolution of the [0 0 1]-oriented nanopillar under compression (D = 8 nm, T = 300 K). Stacking faults bounded by partial dislocations (a) and micro-twins (e) are the main plastic deformation mechanisms, just as the results in Fig. 2.

However, it can be seen that even in the 10 K simulations, dislocation-locking can be overcome in a short time, so that it contributes little to the plastic deformation. At 300 K, stacking faults bounded by partial dislocations and micro-twins are still the main plastic deformation mechanisms for the [0 0 1]-oriented nanopillar, just as the results at 10 K. No significant difference in the plastic deformation mechanisms between the results of 10 and 300 K is observed. The stress fluctuations in the plastic deformation were caused by the formation and annihilation of stacking faults, and such fluctuation manner can be tempered to a certain extent by stacking fault interaction and micro-twin evolution. Since no significant difference exists between the results at 10 and 300 K, in subsequent analyses we will present only the microstructure evolution at 10 K because the deformation mechanisms can be identified more clearly at low temperatures.

Fig. 5 shows the microstructure evolution of the [1 1 1]-oriented nanopillar under compression. Snapshots in Fig. 5a–h are related to the tagged points (A–H) in Fig. 1b. As shown in Fig. 5a–c, six slip systems on three {1 1 1} planes (α, β, γ) nucleate at the surface, which results in the first yield drop at A. The initial dislocation appears in the form of full dislocation loops on {1 1 1} planes. Soon afterwards, more dislocations appear and interact in the pillar (Fig. 5d), corresponding to a region of stress decline in Fig. 1b. As seen in Fig. 5e–g, compressive deformation in the [1 1 1]-oriented nanopillar is mainly accommodated by the nucleation and propagation of full dislocations which finally result in the plastic flow as shown in Fig. 1b. Besides, the full dislocations disappear immediately after reaction, leaving many point defects in the pillar (Fig. 5h).

Fig. 6 shows the microstructure evolution of the [1 1 2]-oriented nanopillar under compression. As is illustrated in Fig. 6a and b, the dislocations nucleate separately on the $(\bar{1}1\bar{1})$ and $(1\bar{1}\bar{1})$ slip planes, and propagate immediately in the pillar. Though dislocations on different slip planes meet with each other (Fig. 6c), strong barriers appearing in the [0 0 1]-oriented nanopillars are not observed. Instead, a stress decline in Fig. 1c occurs. Then dislocations run out of the pillar rapidly, and point defects produced by dislocation interactions are left in the pillar (Fig. 6d and e), and the pillar becomes dislocation-starved. In Fig. 6f, as strain increases, stress builds up again to a new peak till the formation of new dislocations. These new dislocations still glide on $(\bar{1}1\bar{1})$ and $(1\bar{1}\bar{1})$ planes, and undergo the same process of propagation, interaction and annihilation (Fig. 6f and g).

Snapshots of the deformation process of the $[\bar{2}\bar{6}5]$ nanopillar are shown in Fig. 7. These snapshots demonstrate that the [1 1 0] dislocations initially nucleate at surface and then travel through the whole pillar on the $(\bar{1}1\bar{1})$ slip plane (Fig. 7a and b). When reaching the free surface at the opposite end, the dislocations disappear, leaving a surface step (Fig. 7b). Meanwhile, new dislocations along the $[\bar{1}10]$ direction prefer to nucleate at this step, as is shown in the region within the yellow circle. These dislocations glide along the same slip plane, and meet other newly nucleated dislocations (Fig. 7c), and this results in the stress decline in Fig. 1d. Subsequently, as shown in Fig. 7d, the nucleated dislocations run out of the pillar rapidly after

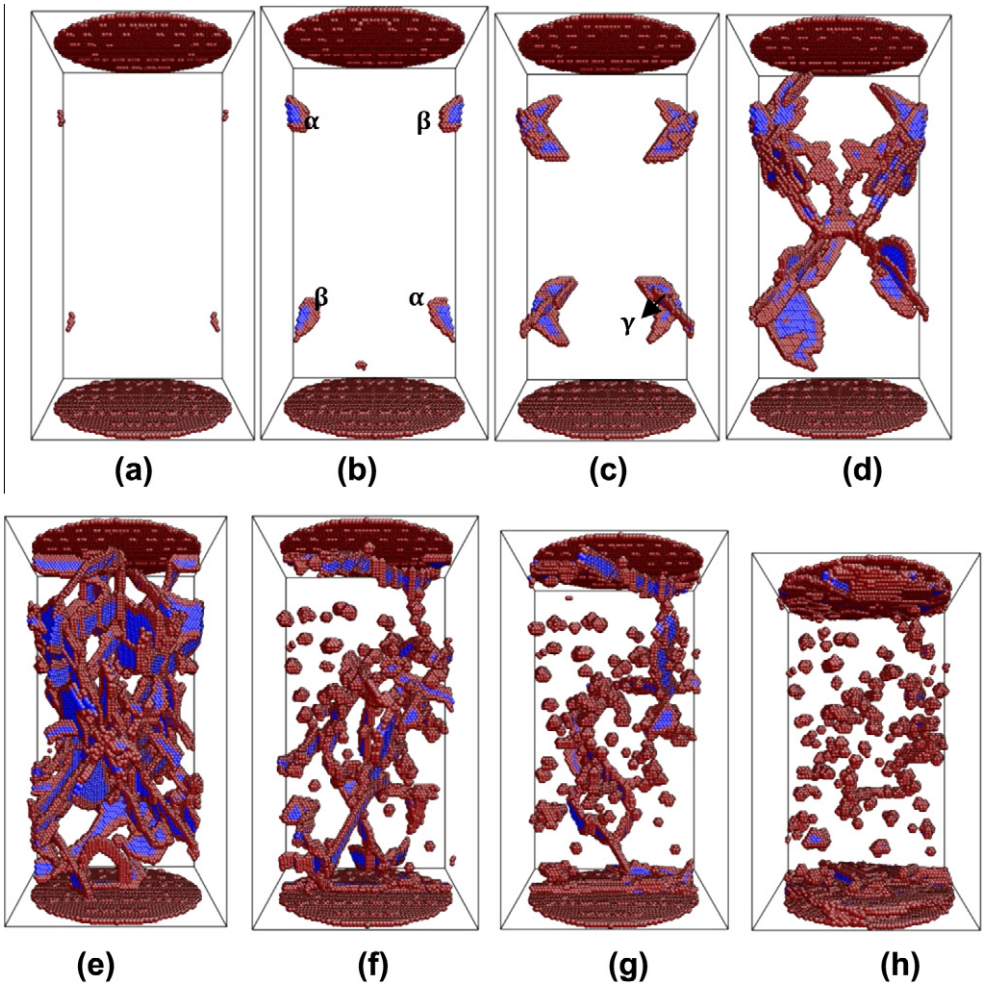

Fig. 5. Snapshots show for the microstructure evolution of the [1 1 1]-oriented nanopillar under compression (T = 10 K). Full dislocations on different {1 1 1} planes nucleation (a–d) and interaction (e–g); the point defects are finally left (h).

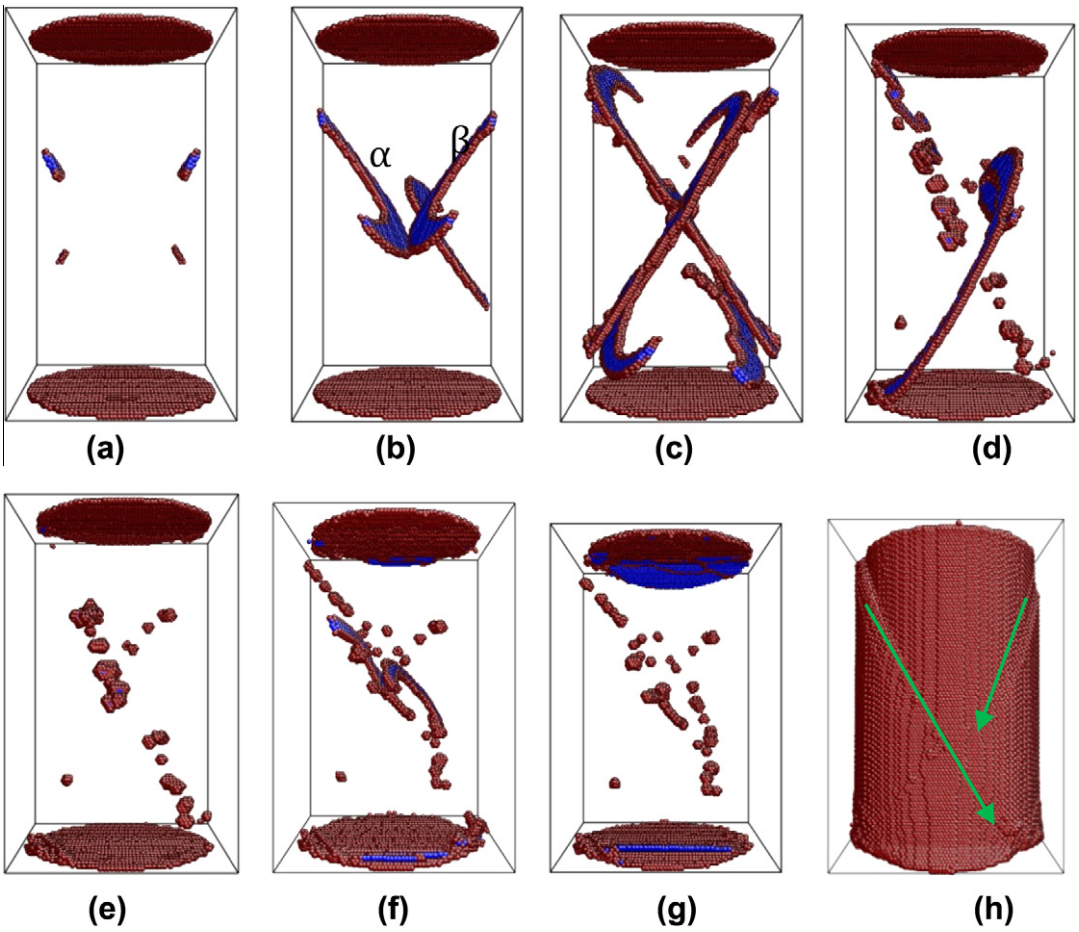

Fig. 6. Snapshots show for the microstructure evolution of the [1 1 2]-oriented nanopillar under compression (T = 10 K). Dislocations nucleate separately along the $(\bar{1}1\bar{1})$ and $(1\bar{1}\bar{1})$ slip planes (a), and interact with each other (b and c). Point defects are left (e) after dislocations run out of the pillar rapidly.

interaction, and the stress builds up again. The dislocation-starved state is similar to that in the [1 1 2]-oriented nanopillar appears. After the formation of new dislocations in Fig. 7e, the stress begins to decline. In Fig. 7g, another dislocation-starved state at a higher strain condition happens.

3.2. Orientation effect on the compressive deformation of nanopillars

From Section 3.1, the fluctuation during the flow phase is somewhat smaller in the [0 0 1] and [1 1 1]-oriented nanopillars than in the [1 1 2] and $[\bar{2}\bar{6}5]$-oriented nanopillars. This is related to the more intensive dislocation interactions in the [0 0 1] and [1 1 1] orientation. In the [0 0 1] orientation, stacking faults on four intersecting slip planes bounded by partial dislocations and micro-twins contribute to the plastic deformation, and the frequent dislocation interactions in this case correspond to a more mean-field environment causing the flow stress to fluctuate less. On the contrary, full dislocations are the primary strain carriers in the [1 1 1], [1 1 2] and $[\bar{2}\bar{6}5]$-oriented nanopillars. This is in agreement with the Schmid law analysis shown in Table 1. Here, the Schmid factors of the leading partial dislocation (m_l) and the trailing partial dislocation (m_t) are evaluated, and if $m_l < m_t$, the trailing partial dislocation should nucleate immediately and catch up with the leading one, so that a full dislocation will form without any extensive stacking fault generated. Otherwise, it will be difficult for the trailing partial dislocation to nucleate, and partial dislocations and stacking faults will appear. In the current work, for the [0 0 1]-oriented nanopillars, partial dislocations are preferred to nucleate and be emitted at the free surface, and it results in the formation of stacking faults and micro-twins. For the [1 1 1], [1 1 2] and $[\bar{2}\bar{6}5]$-oriented nanopillars, however, full dislocations are preferred to nucleate from the free surface, and thus the deformation mechanism is characterized by slip and interactions of full dislocations.

Beside the effects of stacking faults and micro-twins, the number of the primary slip systems also plays an important role in the plastic deformation. In the [1 1 2] and $[\bar{2}\bar{6}5]$-oriented nanopillars, fewer slip systems are activated after the initial yielding. The result is that mobile dislocations can easily escape before complex interactions occur, and so the pillar becomes dislocation-starved quickly. In order to accommodate the deformation, the stress has to be built up again to nucleate new

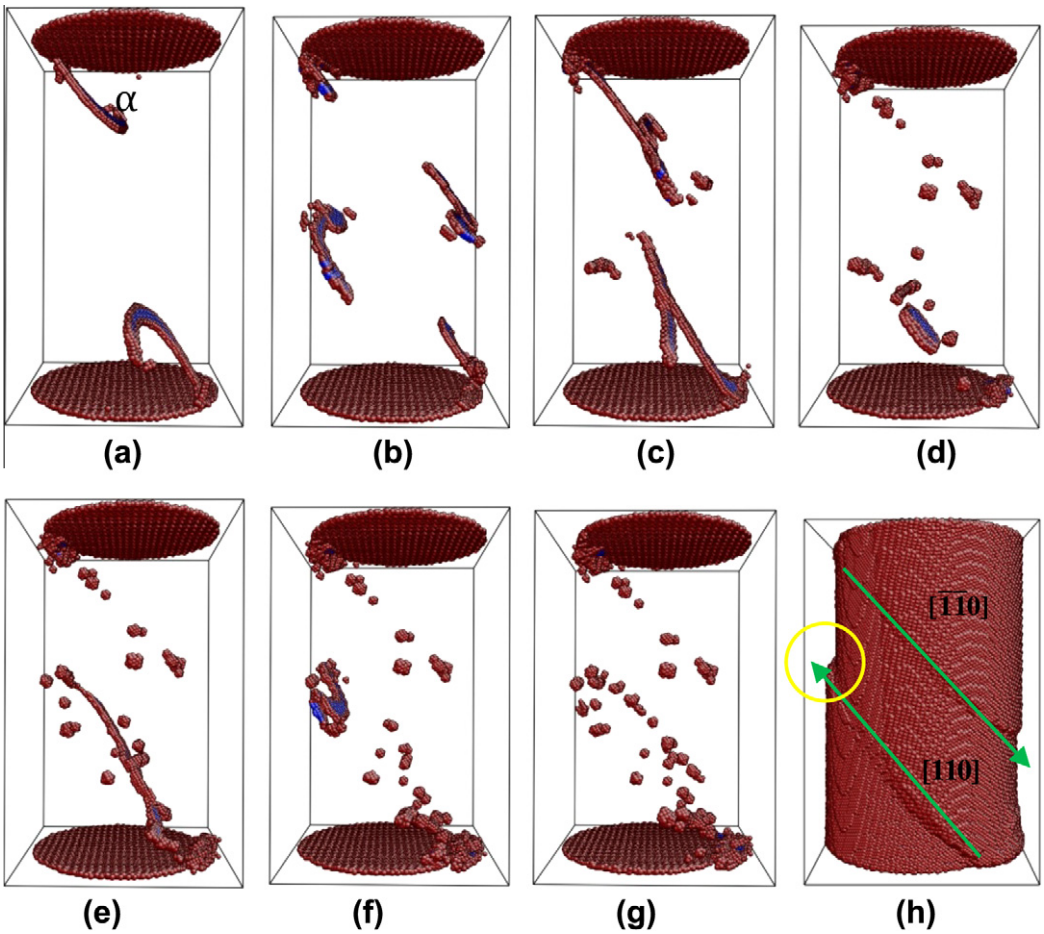

Fig. 7. Snapshots show for the microstructure evolution of the $[\bar{2}65]$-oriented nanopillar under compression ($T = 10$ K). Dislocations nucleate on the $(\bar{1}1\bar{1})$ slip planes (a) and interact (b and c). Point defects are left (d and g) after dislocations run out of the pillar rapidly.

Table 1
Summary of Schmid factor analysis for the deformation mechanisms of different orientation nanopillars.

Orientation/ loading axis	Slip system number	Schmid factor of the leading partial dislocation: m_l	Schmid factor of the trailing partial dislocation: m_t	Predicted mechanism
[001]	8	0.47	0.236	Partial dislocations
[111]	6	0.16	0.31	Full dislocations
[112]	2	0.16	0.31	Full dislocations
$[\bar{2}65]$	1	0.29	0.50	Full dislocations

dislocations, and this process can repeat time after time, corresponding to the serrated strain–stress response. Due to the higher symmetry, there are more primary slip systems in the [001] and [111]-oriented nanopillars, and so dislocations gliding on different planes can meet and react with each other, resulting in different kinds of defects in the pillar. For the [001]-oriented nanopillars, the defects are mostly in the form of dislocation locks and micro-twins, and they serve as obstacles to further dislocation gliding. For the [111]-oriented nanopillars, a number of point defects are created by dislocation interactions. Complex interactions inside the pillar give rise to a higher degree of averaging of stress, resulting in a more mean-field environment of plasticity (Dimiduk et al., 2007). However, dislocations will annihilate at the surface as strain increases for the [001] and [111]-oriented nanopillars. A dislocation-starved state is also observed at a higher strain condition (shown in Fig. 2h and Fig. 3e). It can be concluded from the above discussion that the serrated deformation for nanopillars with different orientations can be understood by dislocation nucleation-controlled mechanisms and the dislocation-starvation hypothesis.

It is worth noting that the nanopillar in our model is defect-free before compression, and this may not be the case in small-scale compression experiments. Thus, we also simulated the compression process for the [001]-oriented nanopillars

with several random vacancies. We found that the high symmetry of the [0 0 1] orientation is partly broken by initial defects, as slip on four different {1 1 1} planes are no longer activated at the same time, and some stacking faults bounded by partial dislocations run out of the pillar before interaction. As a result, the dislocation-starved state is much easier to achieve, corresponding to more serrated deformation. This is in agreement with experimental observations (Greer and Nix, 2006; Greer et al., 2005), and shows that the experimental condition and initial defects in the specimen may also contribute to the jerky and stochastic deformation.

3.3. Size dependence for nanopillars during compressive deformation

Fig. 8 shows the double logarithmic plot of yield strength vs. pillar diameter D for the nanopillars with different orientations. The yield strength is defined as the first peak stress similar to point A in Fig. 1. For all four orientations studied, there is a small size effect on the yield strength approximately obeying a power law $\sigma \propto D^{-m}$, which has been discussed frequently for larger pillars with micron sizes (Greer and Nix, 2006; Greer et al., 2005). However, the exponent value m here in Fig. 8 is much smaller in the range of 0.06–0.21 depending on the compression orientation, compared to the 0.3–1 for the micron sized pillars (Gu and Ngan, 2012). Micron-sized pillars should contain pre-existing dislocations, and Taylor interactions amongst these pre-existing dislocations have been predicted to give rise to a power-law size dependence of strength with m inversely related to the fractal dimension of the initial dislocation network (Ngan, 2011; Gu and Ngan, 2012). Here in Fig. 8, the simulated pillars are nanometer sized with no pre-existing dislocations, and the first yield strength is controlled by dislocation nucleation from free surfaces. The size dependence here is similar to other MD simulation results (Horstemeyer et al., 2001; Zuo and Ngan, 2006; Zuo et al., 2005) where strength is controlled by dislocation nucleation. In the study by Horstemeyer et al., the size effect was given in the form of $\tau_{rss}/\mu = 3.2 \times 10^{-5}(V/A_S)^{-0.38}$ (Horstemeyer et al., 2001), where the stress required to nucleate dislocations from free surfaces was found to scale with a geometric length scale defined by the ratio of volume to surface area of the samples (V/A_S). In the study by Zuo et al., the size dependence arises from the number of potential nucleation sites for new dislocations (Zuo and Ngan, 2006; Zuo et al., 2005), and since a larger pillar should have more of such sites, it should be easier to yield than a smaller pillar.

The plastic stress–strain responses for nanopillars are also analyzed, but for the sake of brevity, we only present the results for the $[\bar{2}65]$ and [0 0 1]-oriented nanopillars here. As illustrated in Fig. 9a, the serrated behavior in low symmetry oriented nanopillars during the flow phase subsides with increasing pillar diameter. When the diameter of the pillar is up to 32.4 nm, the serrated behavior totally disappears. This confirms the proposition that rapid annihilation in small size sample leads to dislocation-starvation in a short time, and finally corresponds to a more intensive serrated flow behavior. In contrast, for nanopillars with higher symmetry orientations as shown in Fig. 9b, no obvious serrated behavior is observed for the samples in different sizes, because more slip systems are activated simultaneously and interact after the initial yielding. Both smaller diameter and fewer slip systems are expected to make the nucleated dislocation glide to the opposite free surface easily, thus inducing the serrated behavior.

In order to test the above proposition, we performed compression simulations for Al nanopillars with a rigid coating outside. This was carried out by forbidding the atoms on the side surface to have radial displacements during the relaxing process between each loading step. In this case, dislocations are not allowed to annihilate on the surface and are therefore confined inside the pillar. Figs. 10 and 11 show the stress–strain responses and the corresponding microstructural evolution, respectively. The lack of free surface in this case prevents dislocation nucleation until a much higher stress is reached, and after such initial yielding, the nucleated dislocations are trapped near the coating. The condition of dislocation-starvation

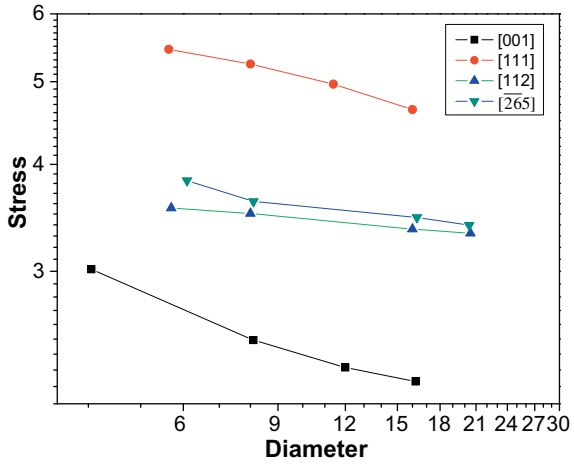

Fig. 8. Log–log plot of yield strength vs. pillar diameter for the nanopillars with different orientations (T = 10 K).

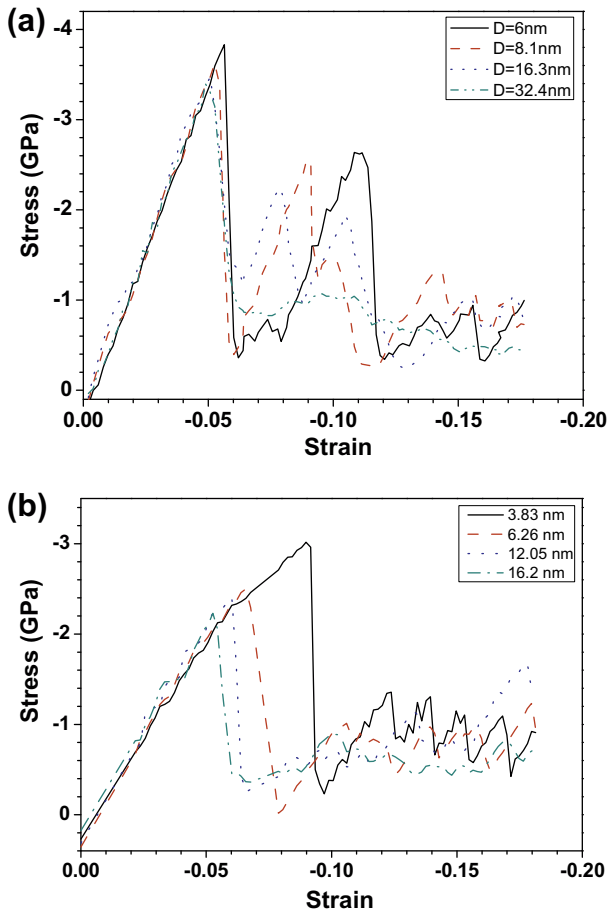

Fig. 9. Stress–strain responses for the nanopillars with different diameters ($T = 10$ K). (a) $[\overline{2}65]$-oriented; (b) [001]-oriented.

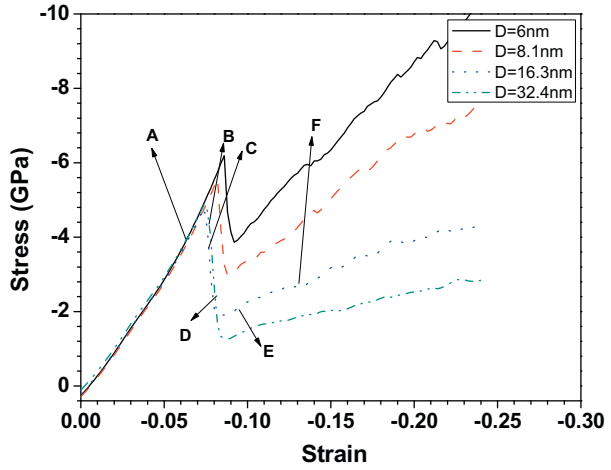

Fig. 10. Stress–strain responses for the $[\overline{2}65]$-oriented nanopillars with rigid coating ($T = 10$ K).

does not occur, and dislocations pile up and interact at the coating, and thus the stress increases with strain in a rather smooth manner without serrations. The simulated results here correspond well to experimental observations of coated Al pillars (Ng and Ngan, 2009b). These results also illustrate that the serrated plasticity behavior in uncoated nanopillars is due to dislocation nucleation and annihilation.

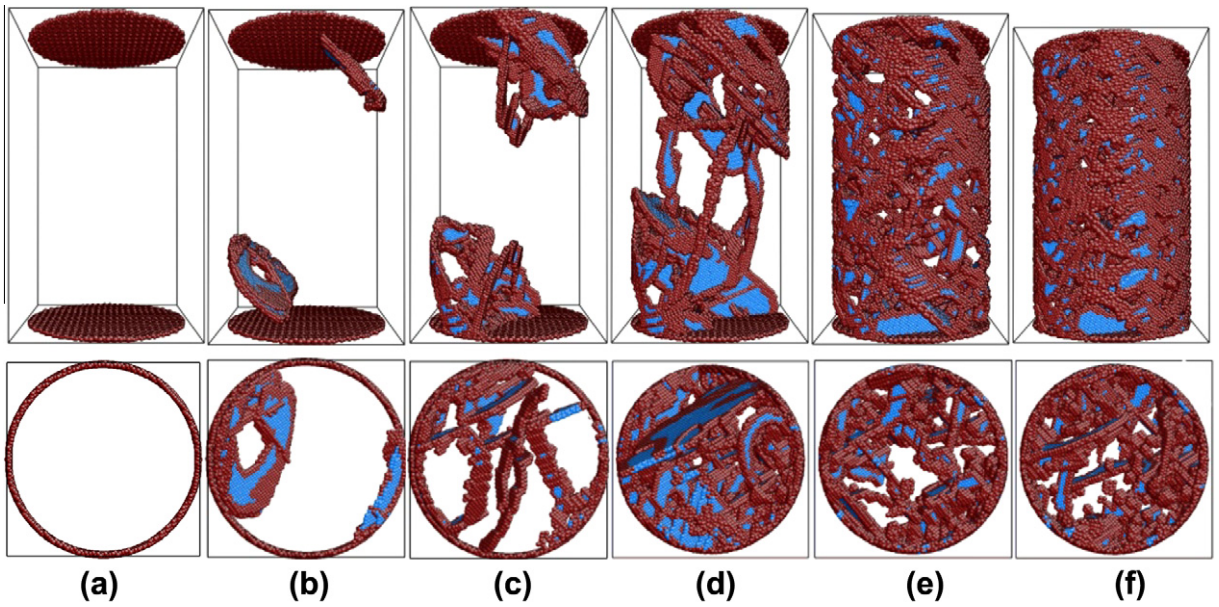

Fig. 11. Snapshots of microstructure viewed from the front and top sides of the $[\overline{2}65]$-oriented nanopillars at different compression strains. Atoms in the coating are not shown while viewed from the front sides. Dislocations nucleate near the coating at a high stress condition (b) and finally pile up at the coating (e and f).

4. Conclusions

Molecular dynamics simulations are applied to study the compression of Al nanopillars with different orientations and sizes. For the four different orientations studied, different plastic deformation mechanisms are observed. In [001]-orientated nanopillars, stacking faults bounded by partial dislocations and micro-twins are the main plastic deformation mechanisms, whereas full dislocations are responsible for the deformation in the [111], [112] and $[\overline{2}65]$-oriented nanopillars. Meanwhile, the number of the primary slip systems plays an important role on the plastic deformation. In the [001] and [111]-orientated nanopillars, more slip systems nucleate at the same time, thus the frequent dislocation interactions lead to smaller fluctuations of the flow stress after the initial yield point which corresponds to the nucleation of the first dislocations. In the [112] and $[\overline{2}65]$-oriented nanopillars, fewer slip systems are activated after the initial yielding leading to the easy achievement of the dislocation-starved condition, and thus the post-yield flow response is more severely fluctuating and serrated. The serrated plastic deformation can be well explained by whether the dislocation processes can lead to a dislocation-starved state. This is further confirmed by simulations on coated pillars, when dislocations produced are now trapped by the coating, and smooth rather than serrated deformation occurs corresponding to the frequent interactions in a mean-field manner. In addition to size which is a well-known effect, both the orientation and dislocation confinement condition of the pillar have a significant influence on dislocation propagation, interaction and annihilation, and consequently the plastic deformation.

Acknowledgments

This work was supported by Chinese Nature Science Foundation (Project No. 11072026). S. Xu's visit to HKU was supported by a grant from the Hong Kong Research Grants Council (Project No. 7159/10E).

References

Akarapu, S., Zbib, H.M., Bahr, D.F., 2010. Analysis of heterogeneous deformation and dislocation dynamics in single crystal micropillars under compression. Int. J. Plasticity 26, 239–257.
Cao, A., Ma, E., 2008. Sample shape and temperature strongly influence the yield strength of metallic nanopillars. Acta Mater. 56, 4816–4828.
Diao, J., Gall, K., Dunn, M.L., Zimmerman, J.A., 2006. Atomistic simulations of the yielding of gold nanowires. Acta Mater. 54, 643–653.
Dimiduk, D.M., Uchic, M.D., Rao, S.I., Woodward, C., Parthasarathy, T.A., 2007. Overview of experiments on microcrystal plasticity in FCC-derivative materials: selected challenges for modelling and simulation of plasticity. Model. Simul. Mater. Sci. Eng. 15, 135–146.
El-Awady, J.A., Rao, S.I., Woodward, C., Dimiduk, D.M., Uchic, M.D., 2011. Trapping and escape of dislocations in micro-crystals with external and internal barriers. Int. J. Plasticity 27, 372–387.
Greer, J.R., Nix, W.D., 2006. Nanoscale gold pillars strengthened through dislocation starvation. Phys. Rev. B 73.
Greer, J.R., Oliver, W.C., Nix, W.D., 2005. Size dependence of mechanical properties of gold at the micron scale in the absence of strain gradients. Acta Mater. 53, 1821–1830.

Gu, R., Ngan, A.H.W., 2012. Dislocation arrangement in small crystal volumes determines power-law size dependence of yield strength. Journal of the Mechanics and Physics of Solids, in press, http://dx.doi.org/10.1016/j.jmps.2012.10.002.
Honeycutt, J.D., Andersen, H.C., 1987. Molecular dynamics study of melting and freezing of small Lennard-Jones clusters. J. Phys. Chem. 91, 4950–4963.
Horstemeyer, M.F., Baskes, M.I., Plimpton, S.J., 2001. Length scale and time scale effects on the plastic flow of fcc metals. Acta Mater. 49, 4363–4374.
Jang, D., Gross, C.T., Greer, J.R., 2011. Effects of size on the strength and deformation mechanism in Zr-based metallic glasses. Int. J. Plasticity 27, 858–867.
Kang, K., Cai, W., 2010. Size and temperature effects on the fracture mechanisms of silicon nanowires: molecular dynamics simulations. Int. J. Plasticity 26, 1387–1401.
Kim, J.-Y., Jang, D., Greer, J.R., 2012. Crystallographic orientation and size dependence of tension–compression asymmetry in molybdenum nano-pillars. Int. J. Plasticity 28, 46–52.
Korte, S., Barnard, J.S., Stearn, R.J., Clegg, W.J., 2011. Deformation of silicon – insights from microcompression testing at 25–500°C. Int. J. Plasticity 27, 1853–1866.
Kunz, A., Pathak, S., Greer, J.R., 2011. Size effects in Al nanopillars: single crystalline vs. bicrystalline. Acta Mater. 59, 4416–4424.
Li, J., 2003. AtomEye: an efficient atomistic configuration viewer. Model. Simul. Mater. Sci. Eng. 11, 173.
Li, X.Y., Yang, W., 2009. Size dependence of dislocation-mediated plasticity in Ni single crystals: molecular dynamics simulations. J. Nanomater..
Liu, Q., Shen, S., 2012. On the large-strain plasticity of silicon nanowires: effects of axial orientation and surface. Int. J. Plasticity 38, 146–158.
Liu, Z.L., Liu, X.M., Zhuang, Z., You, X.C., 2009. A multi-scale computational model of crystal plasticity at submicron-to-nanometer scales. Int. J. Plasticity 25, 1436–1455.
Ng, K.S., Ngan, A.H.W., 2008. Stochastic nature of plasticity of aluminum micro-pillars. Acta Mater. 56, 1712–1720.
Ng, K.S., Ngan, A.H.W., 2009a. Deformation of micron-sized aluminium bi-crystal pillars. Philos. Mag. 89, 3013–3026.
Ng, K.S., Ngan, A.H.W., 2009b. Effects of trapping dislocations within small crystals on their deformation behavior. Acta Mater. 57, 4902–4910.
Ngan, A.H.W., 2011. An explanation for the power-law scaling of size effect on strength in micro-specimens. Scripta Mater. 65, 978–981.
Park, H.S., Gall, K., Zimmerman, J.A., 2006. Deformation of FCC nanowires by twinning and slip. J. Mech. Phys. Solids 54, 1862–1881.
Plimpton, S., 1995. Fast parallel algorithms for short-range molecular dynamics. J. Computat. Phys. 117, 1–19.
Rabkin, E., Nam, H.S., Srolovitz, D.J., 2007. Atomistic simulation of the deformation of gold nanopillars. Acta Mater. 55, 2085–2099.
Rao, S.I., Dimiduk, D.M., Parthasarathy, T.A., Uchic, M.D., Tang, M., Woodward, C., 2008. Athermal mechanisms of size-dependent crystal flow gleaned from three-dimensional discrete dislocation simulations. Acta Mater. 56, 3245–3259.
Shan, Z.W., Mishra, R.K., Asif, S.A.S., Warren, O.L., Minor, A.M., 2008. Mechanical annealing and source-limited deformation in submicrometre-diameter Ni crystals. Nature Mater. 7, 115–119.
Uchic, M.D., Dimiduk, D.M., Florando, J.N., Nix, W.D., 2004. Sample dimensions influence strength and crystal plasticity. Science 305, 986–989.
Uchic, M.D., Shade, P.A., Dimiduk, D.M., 2009. Plasticity of micrometer-scale single crystals in compression, Ann. Rev. Mater. Res. Annual Reviews, Palo Alto, pp. 361–386.
Voter, A.F., Chen, S.P., 1987. Accurate interatomic potentials for Ni, Al and Ni3Al. MRS Proc. 82, 175–180.
Wang, Z.J., Li, Q.J., Shan, Z.W., Li, J., Sun, J., Ma, E., 2012. Sample size effects on the large strain bursts in submicron aluminum pillars. Appl. Phys. Lett. 100.
Wang, Z.Q., Beyerlein, I.J., LeSar, R., 2009. Plastic anisotropy in fcc single crystals in high rate deformation. Int. J. Plasticity 25, 26–48.
Weinberger, C.R., Battaile, C.C., Buchheit, T.E., Holm, E.A., 2012a. Incorporating atomistic data of lattice friction into BCC crystal plasticity models. Int. J. Plasticity 37, 16–30.
Weinberger, C.R., Jennings, A.T., Kang, K., Greer, J.R., 2012b. Atomistic simulations and continuum modeling of dislocation nucleation and strength in gold nanowires. J. Mech. Phys. Solids 60, 84–103.
Yoo, B.-G., Kim, J.-Y., Kim, Y.-J., Choi, I.-C., Shim, S., Tsui, T.Y., Bei, H., Ramamurty, U., Jang, J.-i., 2012. Increased time-dependent room temperature plasticity in metallic glass nanopillars and its size-dependency. Int. J. Plasticity 37, 108–118.
Zhu, T., Li, J., Samanta, A., Leach, A., Gall, K., 2008. Temperature and strain-rate dependence of surface dislocation nucleation. Phys. Rev. Lett. 100.
Zuo, L., Ngan, A.H.W., 2006. Molecular dynamics study on compressive yield strength in Ni3Al micro-pillars. Philos. Mag. Lett. 86, 355–365.
Zuo, L., Ngan, A.H.W., Zheng, G.P., 2005. Size dependence of incipient dislocation plasticity in Ni3Al. Phys. Rev. Lett. 94.